CrossMark

A Desktop Tensile Kolsky Bar for the Dynamic Testing of Metallic Foils

Jastin V. Paul[1] · Jamie Kimberley[1,2]

Abstract A miniature tension Kolsky (split-Hopkinson) bar has been developed to facilitate measurement of the uniaxial stress–strain constitutive response of metallic foils at strain rates on the order of 10^4 s^{-1}. The system utilizes a cylindrical launch tube with an internal striker to generate the loading pulse. This launch tube set-up allows for the use of traditional disk shaped pulse shapers which may be required to ensure that the specimen in deformed under force equilibrium and at a nearly constant strain rate. Unlike most traditional Kolsky bar systems, incident and transmitted bars with rectangular cross-section are used to facilitate specimen and strain gage mounting. The rectangular bar cross-section also provides a reduced cross sectional bar area when compared to an equivalent diameter circular section which increases the system sensitivity. The system was used to perform dynamic tests on 99.9 % magnesium specimens, illustrating the ability to measure the high-rate response of ductile metals under equilibrium and constant strain rate conditions.

Keywords Dynamic testing · Kolsky · Slit Hopkinson · Strain rate · Foil

✉ Jamie Kimberley
jamiek@nmt.edu

1 Department of Mechanical Engineering, New Mexico Institute of Mining and Technology, Socorro, NM, USA

2 Energetic Materials Research and Testing Center, New Mexico Institute of Mining and Technology, Socorro, NM, USA

Introduction

Mechanical material properties such as yield stress and ultimate strength are most commonly obtained under quasi-static loading conditions, however most classes of materials including metals, ceramics, and polymers exhibit significant changes in mechanical response when subjected to loading at elevated strain rates. The strain rate at which a specimen is deformed can affect the response of critical material properties such as elastic modulus, yield strength, work hardening, and ductility. The loading strain rate may also affect the failure mechanisms activated. To ensure product quality and reliability under high strain rate loading conditions (e.g. impact, metal forming), the mechanical responses of materials under dynamic loading conditions must be characterized. Many testing techniques have been developed to perform these dynamic measurements, with the Kolsky bar [1] (also known as split-Hopkinson pressure bar) being the most commonly employed technique to measure the uniaxial compressive constitutive behavior of materials under high strain rates (10^2 –10^5 s^{-1}).

In addition to strain rate dependence, material response may depend on the state of stress under which the deformation occurs. In ductile polycrystalline metals this anisotropic response is often a manifestation of preferred orientation or texture in the material grain structure. This is especially true for metals with low symmetry crystal structure, e.g. hexagonal close packed, which often exhibit anisotropic elastic and plastic response when the individual grains of the aggregate are preferentially aligned or highly textured [2]. The failure response may also be sensitive to the stress state with compressive states promoting failure by shear banding, and tensile states promoting void growth, or fracture.

The combined effects of loading rate and stress state sensitivity have led to the development testing techniques

that probe the dynamic response of materials under various stress states. Many of these are adaptations of the original compressive Kolsky bar, and include the torsional Kolsky bar for testing materials under shear (e.g., [3]), the tensile Kolsky bar for dynamic tensile testing (e.g., [4]), as well as systems capable of subjecting specimens to combined loading e.g. compression-torsion [5].

Another critical development in high rate material testing was the miniaturization of the compressive Kolsky bar often referred to as a desktop Kolsky bar [6]. By reducing the size of the system and specimen, higher strain rates could be achieved because strain rate is inversely proportional to the specimen length. This reduction in specimen size has other benefits like the ability to test materials such as nanocrystalline metals that may not be available in bulk, and the ability to visualize specimen deformation as length scales on the order of the material microstructure. These desktop techniques have been adapted to tensile testing of fibers/filaments [7], and very recently metal films [8].

The objective of this work is to develop a miniature tension-Kolsky bar to perform small-scale dynamic tensile tests. Using specimens with gage lengths of the order of 1 mm will increases the attainable strain rates up to 10^4 s^{-1} as compared with the strain rates of 10^2–10^3 s^{-1} that are typically achieved in traditional tensile Kolsky bar tests. Design considerations for incorporating the latest advances in large scale Kolsky testing as well as an evaluation of diagnostics will be discussed. Lastly, dynamic tensile test results are presented for Magnesium foils.

Overview of Kolsky Bar Testing and Analysis

Despite the development of many variants of the original compression Kolsky bar technique, all of these systems rely on the fundamentals of one-dimensional elastic wave propagation in the bars to determine the stress, strain rate, and strain as functions of time in the deforming specimen. Here, a brief recap is provided of the critical assumptions and equations of Kolsky bar analysis presented in the context of classical compression testing. The reader is encouraged to read the excellent review articles [9, 10] for a more thorough treatment of the subject.

Consider a specimen located between two slender elastic rods. An incident strain pulse ε_i travels in the incident bar toward the specimen. Upon reaching the specimen the part of this strain pulse is transmitted through the specimen into the transmitted bar ε_t and a portion is reflected back into the incident bar ε_r. These strain pulses can be measured by the strain gages mounted to the surface of the bars. The measured strain pulses and one-dimensional wave propagation arguments can be used to determine the normal forces at the incident bar/specimen interface,

$$P_{inc}(t) = E_b(\varepsilon_I + \varepsilon_R)A_b, \tag{1}$$

and the transmitted bar/specimen interface

$$P_{tran}(t) = E_b\varepsilon_T A_b. \tag{2}$$

The average engineering stress in the specimen is then given by,

$$\sigma_s = \frac{P_{inc} + P_{tran}}{2}\frac{1}{A_{s0}} = \frac{E_b}{2}\frac{A_b}{A_{s0}}(\varepsilon_I + \varepsilon_R + \varepsilon_T) \tag{3}$$

where A_{s0} is the initial cross-sectional area of the specimen, E_b is the elastic modulus of the bars, A_b is the cross sectional area of the bars, A_s is the cross sectional area of the sample.

If the specimen is under state of force equilibrium ($P_{inc} = P_{tran}$) then, $\varepsilon_I + \varepsilon_R = \varepsilon_T$ and the engineering stress in the specimen is

$$\sigma_s(t) = \frac{E_b A_b}{A_{s0}}\varepsilon_T(t). \tag{4}$$

Following a similar process to calculate the velocities at the specimen/bar interfaces and assuming that the specimen is in equilibrium, the engineering strain rate in the specimen is

$$\dot{\varepsilon_s}(t) = -\frac{2c_b}{l_0}\varepsilon_R(t). \tag{5}$$

Here, l_o is the initial length of the specimen, $c_b = \sqrt{E_b/\rho_b}$ is the elastic wave speed of the bar where ρ_b is the mass density of the bars. The strain in the specimen can then be calculated by integrating Eq. (5) with respect to time.

Description of Experimental Set-up

This section presents the details of the newly developed miniature tensile Kolsky bar experimental setup. The bar was developed adapting tensile Kolsky bar designs that utilize a hollow launch tube with internal striker [11, 12] to small-scale material testing in a manner similar to the miniaturization of a compression Kolsky bar by [6]. The Kolsky bar consists of three major components: a loading device (gas chamber, launch tube and cylindrical striker), bar components (incident and transmitted bar), and support structure as shown in Fig. 1. The loading device and the bar components are secured to a 910 mm (36 in) aluminum beam with a central V-groove using circular brass bushings. The V-groove is machined to maintain deviations in straightness and flatness to below ±0.005 mm which keeps the loading device and the bar components secure and aligned to a common axis, The brass bushings were machined to outside diameter tolerance of ±0.005 mm.

Fig. 1 Schematic showing the assembled components of a miniature tensile Kolsky bar
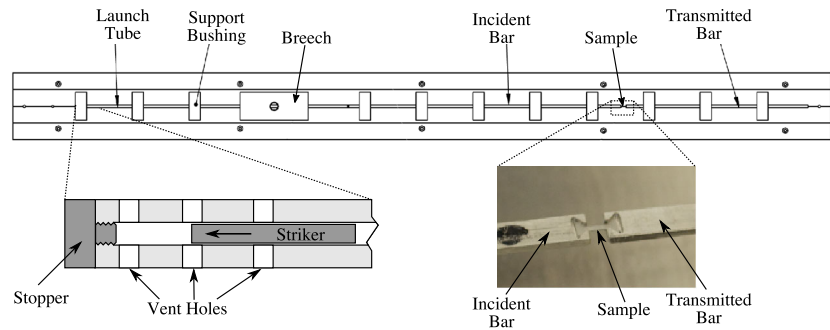
The specific location of bushings was selected to allow the bars to translate along this axis with minimal friction.

The main components of the loading device consist of the gas chamber, launch tube, and a striker. The main body of the gas chamber is a hollow cylinder with a internal diameter of 12.7 mm (0.5 in) and an outside diameter of 31.75 mm (1.25 in). Cover plates that include o-ring glands to seal the plate/body and plate/launch tube interfaces are attached to both ends of the body of the gas chamber. The launch tube is a hollow 6061-T6 aluminum tube (Vita-needle) 305 mm (12.375 in) in length and has an outside diameter of $3.175^{+0.10}_{-0.05}$ mm (0.125 in) and an inside diameter of 1.65 ± 0.16 mm (0.065 in). It is worth noting that the tolerances are specified by the manufacturer, and the actual variation on our tube was significantly lower. The striker is a steel cylindrical plug gage with a diameter of $1.574^{+0.000}_{-0.005}$ mm (0.062 in) which slides freely inside the launch tube. The cross-sectional dimensions and materials of the striker and launch tube were selected so that the acoustic impedances of the striker and launch tube were identical, i.e. $(\rho cA)_{tube} = (\rho cA)_{striker}$, where ρ is the mass density, c is the elastic bar wave speed, and A is cross sectional area. For the materials and values selected here there is a 1 % difference between the impedances of the striker and launch tube, ensuring complete wave transfer from the striker to the launch tube.

To generate the loading pulse for testing, compressed air is transferred into the gas chamber using a fast-acting solenoid valve. The pressurized air flows from the chamber into the launch tube via a machined opening in the launch tube and propels the striker down a hollow launch tube until it impacts a stopper at the end of launch tube. The stopper is a machine screw that has been polished flat on the impact face. The impact of the striker on the stopper generates a compressive wave that reflects from the free end of the stopper as a tensile wave ϵ_i that travels down the launch tube as can be seen in the closeup view of the stopper end of the launch tube in the left inset of Fig. 1. Vent holes are drilled on the end of the launch tube near the stopper to ensure that the striker speed is not reduced by an air cushion effect. These vent holes also allow for the impact velocity to be determined by measuring the time of flight between photo gates positioned across the holes.

The incident and transmitted bars are made out of 2024-T4 aluminum and have lengths of 314 and 203 mm, respectively. This aluminum alloy was selected for its high yield strength (bars must remain elastic during testing) and because the value of Young's modulus (70 GPa) provides better system sensitivity as compared to steel (210 GPa) when strain gages are used for measuring the strain in the bars. The incident and transmitted bars were manufactured on a standard milling machine, using soft jaws that were purpose built to ensure dimensional accuracy. The incident bar is connected to the launch tube via a threaded connection (3-48 UNF thread, 10 mm of engagement) at one end allowing for the transmission of the tensile loading wave into the incident bar. The incident and transmitted bars have a rectangular cross-section of 3.2 ± 0.002 mm width by 1 ± 0.002 mm height. Ideally this cross section would be selected so that the bars were impedance matched to the launch tube to simplify the wave propagation in the system. Limitations of commercially available components (e.g. launch tube), manufacturing challenges (requirement for enough material to cut threads, suffcent material to facilitate specimen attachment), and system sensitivity considerations (incident and transmitted bar dimensions) resulted in a mismatch of impedance that results in the strain pulse transmitted into the incident bar being 1.29 times the strain pulse in the launch tube. It should be possible to create a system where all components are impedance matched, but to manufacture a system where the even the connection between the launch tube and incident bar are impedance matched would require significantly more machining and most likely the use of a permanent connection between these components. This is a possible refinement that may affect the rise time of the loading pulse in the system, which is discussed later in the manuscript.

The use of a rectangular cross-section provides several benefits when compared with traditional bars of circular cross-section. First, it results in increased measurement sensitivity in the transmitted bar when compared with a

circular cross section of diameter equal to the width of the rectangular section because of the reduced cross-sectional area. Second, the rectangular section provides flat surfaces which aid in the mounting of strain gages. Finally, the flat surfaces and associated bushings resist rotation about the axis of the bar which would be problematic when testing thin foil specimens, as is the case in this work.

The tensile test specimens are shaped like a dog bone and are milled from flat sheets of material using a micro-mill. Figure 2 shows the dimensions of a specimen with 1 mm gage length. The gage width is 0.5 mm and the specimen thickness is approximately 0.2 mm. The angle of the grip section and the fillet radius between the grip and the gage sections are 135° and 0.5 mm, respectively. To grip the specimens during testing, pockets matching the dimensions of the grip section of the samples were machined directly into the ends of the incident and transmitted bar as shown in the right inset of Fig. 1. The pockets were milled directly into the bar to minimize disturbances to the wave profiles that may result if bulky external grips or specimens that are threaded directly into the bars are used [12].

Traditional Kolsky bar analysis utilizes the strain measured in the incident and transmitted bars along with one-dimensional elastic wave propagation arguments to determine the state of stress, strain rate, and strain in the specimen. The strain pulses in the incident and transmitted bars are typically measured using metal foil strain gages. The small size of miniature Kolsky bar systems and the low force levels associated with small samples often precludes the use of metal foil gages, forcing researchers to use alternatives such as optical interferometer techniques [13], quartz stress gages/load cells [7], or semiconductor strain gages to measure the strain (or equivalent) in the incident and transmitted bars. Our system utilizes semiconductor strain gages to measure the bar strains allowing for the traditional Kolsky bar analysis to be utilized. These gages have a small footprint allowing them to be mounted easily
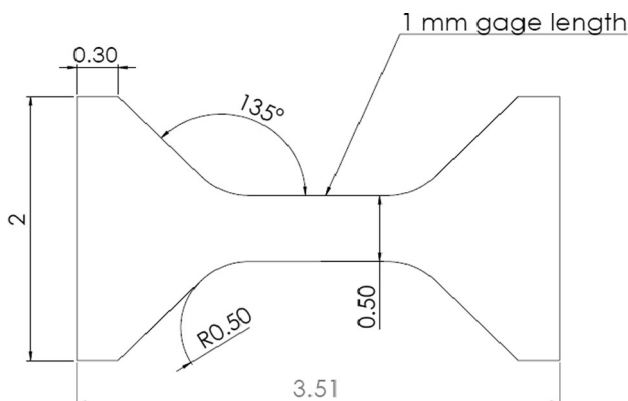
to or flat bars. The gages also have a gage factor $S_g = 155$, that is $75\times$ higher than a typical metal foil gage, resulting in increased strain sensitivity. The gages also have a small active gage length providing high temporal resolution. Gages are mounted to the upper and lower surfaces of the incident and transmitted bars at a distance of 144.5 and 43.5 mm from the specimen, respectively. The output of the strain gages mounted to the incident bar were recorded using a constant-voltage potentiometer circuit consisting of a voltage sources, ballast resistor ($R_b = 66$ kΩ) with the two gages ($R_g = 1.05$ kΩ) connected in series. Connecting the active gages in series tends to amplify axial strains and suppress strains that result from bending. The change in voltage measured across the active gages in terms of the applied axial strain ε and excitation voltage E_{0p} is

$$\Delta E_{out} = \frac{r}{(1+r)^2} 2 S_g \varepsilon (1 - n_p) E_{0p}, \tag{6}$$

where $r = \frac{R_b}{2R_g}$ [14]. The non-linear correction term $n_p = 1 - \frac{1}{1+\frac{1}{(1+r)}2S_g\varepsilon}$ is less than 1 % for the selected gages and strain levels in the incident bar (~ 1000 microstrain), and can be ignored in our case.

To measure the strain pulses in the transmitted bar a Wheatstone bridge circuit with two active gages arranged to cancel bending strains was used. This circuit provides increased sensitivity compared to the constant voltage potentiometer circuit. This sensitivity is required to measure the small strains in the transmitted bar that result for the low force levels in the test specimen. The voltage output of the half bridge circuit is

$$E_{out} = \frac{1}{2} E_{0w} S_g \varepsilon (1 - n_w). \tag{7}$$

Here, E_{0w} is the excitation voltage and $n_w = \frac{S_g\varepsilon}{2+S_g\varepsilon}$ is the correction for non-linearity [14]. The nonlinearity term n_w is ~ 0.2 % for the low strain levels measured in the transmitted bar (~ 25 microstrain).

The voltages corresponding to the recorded strain pulses for a test using a 101.6 mm (4 in) striker length are shown as a function of time in Fig. 3. Here, a positive voltage corresponds to a positive strain in the gages. The excitation voltage of the potentiometer circuit for the incident gages E_{0p} was 20 V, and the excitation voltage for the Wheatstone bridge circuit for the transmitted bar E_{0w} was 5 V. Both the incident and transmitted signals have magnitudes on the order of 10's of milivolts and have good signal to noise ratio.

Testing of Magnesium Foils

The capabilities of the minitension bar are demonstrated by presenting results of dynamic tensile tests performed on magnesium samples. Details of the material characteristics

Fig. 2 Dimensioned drawing of the dog-bone shaped specimens used for the minitension Kolsky bar
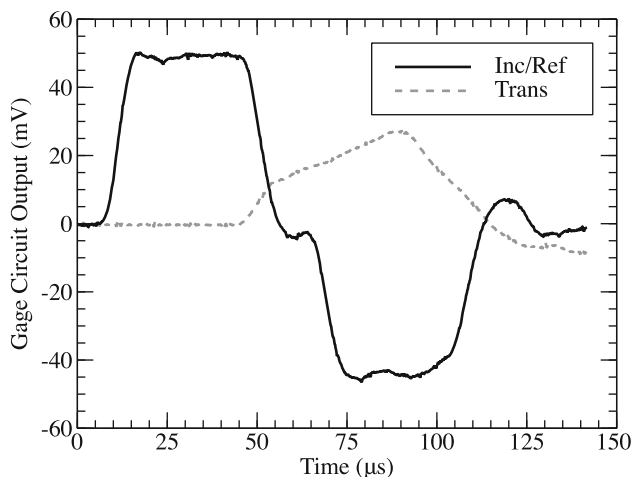
Fig. 3 Voltage signals from the strain gage circuits attached to the incident and transmitted bars plotted with respect to time

(e.g. texture, grain size), sample preparation, and experimental observations of the mechanical response are presented in the following subsections.

Material Description

Billets of 99.9 % Magnesium were processed using equal channel angular extrusion (ECAE) via four passes of the B_c route as described by [15]. The processing route involves extruding a material through a die with a 90° bend as shown in Fig. 4 and provides control over grain size and crystallographic texture of the processed material. The resulting material has nearly equiaxed grains with a mean grain size of 9 μm [16]. The processed material is also

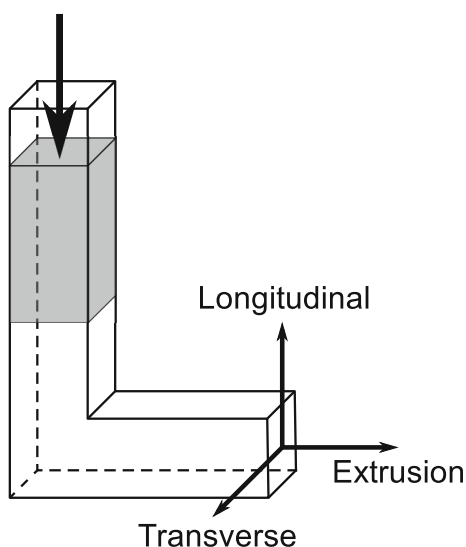strongly textured with the basal poles inclined at roughly 45° to all three directions (detailed analysis of the specimen texture is not presented here for sake of brevity).

The processed billets are then cut into sheets ~1 mm thick using a low speed diamond saw. Individual sheets are then lapped and polished on both sides to a final thickness for testing (~0.2 mm in this case). Dog-bone specimens (Fig. 2) are then cut from the sheets. In the case of this work, the loading axis was aligned with the Extrusion direction, and the surface normal of the specimen was aligned to the Longitudinal direction.

Dynamic Tensile Flow Stress Measurements

Specimens prepared in the manner described above were subjected to dynamic tensile loading using the desktop tension Kolsky bar. The raw voltage signals measured from the strain gage circuits were converted to strain pulses via Eqs. (6) and (7). Force equilibrium in the specimen was verified by plotting P_{inc} and P_{tran} as functions of time as can be found in Fig. 5. Here we observe that the forces come into agreement ~10 μs after the force at the transmitted bar/specimen begins to rise. [17] showed that force equilibrium is established in plastically deforming metallic specimens in the time that it takes for a plastic wave to transit the specimen 3 (actually π) times. Gray [10] followed this analysis and showed that the time to achieve force balance in the specimen is given by

$$t_{eq}^2 = \frac{\pi^2 \rho_s l_0}{\partial \sigma / \partial \epsilon}, \tag{8}$$

where ρ_s is the specimen mass density, and $\partial \sigma / \partial \epsilon$ is the slope of the plastic stress–strain curve. For the specimens with a gage length of 1 mm tested here, it is predicted that
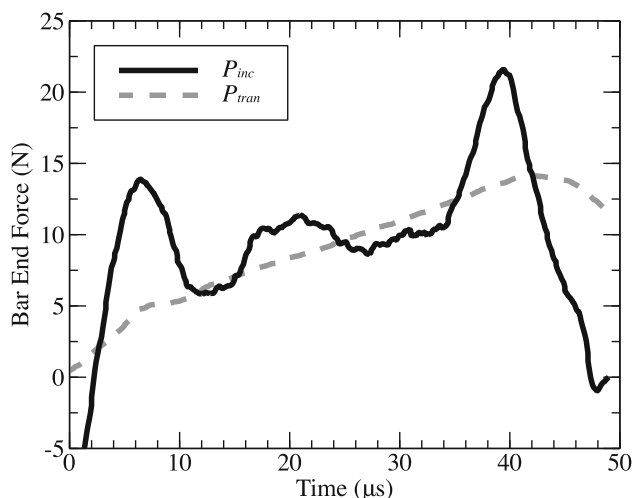

Fig. 4 Schematic of ECAE process geometry including definitions of the three orthogonal directions associated with the process

Fig. 5 Force at the incident bar/specimen (P_{inc}) and transmitted bar/specimen (P_{tran}) interfaces plotted as a function of time

444

J. dynamic behavior mater. (2015) 1:439–446

equilibrium would be established in approximately 7 μs. This compares well with the observed time it takes to achieve force balance in our experiments. The slightly longer time to establish equilibrium measured here results from the fact that P_{inc} is initially negative which is non-physical and likely caused by the small "bump" observed at the leading edge of the reflected pulse denoted by the arrow in Fig. 3. Analysis of an $x - t$ (Lagrangian) diagram of the system indicated that the disturbance at the beginning of the reflected pulse is likely a transverse wave generated at the threaded connection between the launch tube and the incident bar. This transverse wave would have minimal effect on the axial stress in the sample giving confidence that equilibrium is established before the ~ 8 to 10 μs typically observed in these experiments.

Having established that the specimen is deforming under conditions of force equilibrium the strain rate in the specimen as calculated by Eq. (5) is plotted as a function of time in Fig. 6. The strain rate rises to a peak value of 5000 s^{-1} at ~ 6 μs and then shows a slight decrease to a nearly constant value of 4800 s^{-1} until 40 μs when there is a rapid decrease, denoting unloading of the sample. This illustrates that the specimen in being deformed at a nearly constant strain rate of ~ 5000 s^{-1} throughout the duration of the deformation. The strain-rate–time curve can be integrated providing the specimen stain as a function of time. The specimen stress as a function of time can be calculated using Eq. 4, and the resulting stress–strain curve is shown in Fig. 7 along with the results of a sample deformed at 10,000 s^{-1}. We observe little difference between the two curves indicating that rate effects are negligible over the range of strain rates presented. For the specimen deformed at a strain rate of 5000 s^{-1}, the stress–strain data below 3 % strain corresponds to the region of the experiment when equilibrium is not established and the strain rate has not achieved a constant value, accordingly,
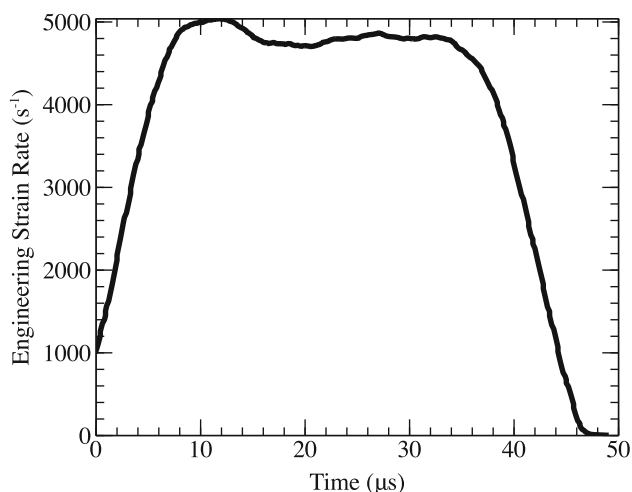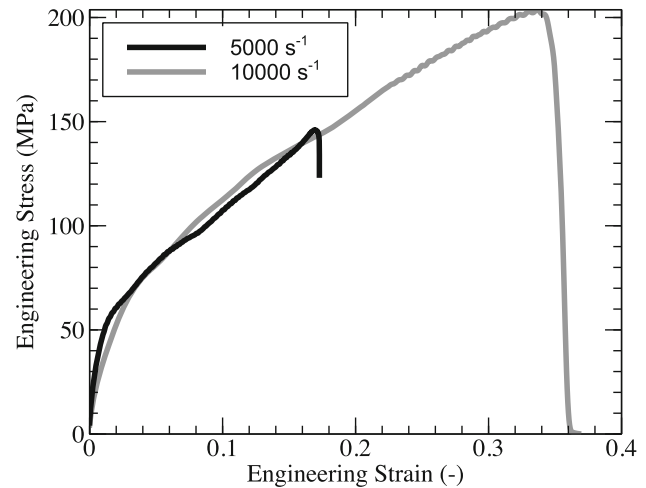

Fig. 7 Engineering stress–strain curves of samples loaded at a strain rates of 5000 and 10,000 s^{-1}. For these particular samples we observe little rate dependence in the range of 5000–10000 s^{-1}

data from this region should not be relied upon. The flow stress measured at ~ 3 % strain is ~ 70 MPa illustrating that the test system has the ability to accurately measure the stress levels of relatively low strength metals. The flow stress shows nearly linear hardening to a level of 150 MPa at 17 % strain at which point the specimen failed and the stress rapidly drops to zero. Similar behavior is observed in the specimen deformed at 10,000 s^{-1}, but the specimen continues to strain up to 34 % strain and a corresponding stress of 200 MPa before unloading.

Discussion of System Range of Operations

While this system was designed with specific material testing requirements in mind, it is certainly capable of being extended for use to characterize other materials and specimen geometries. Practical limits related to material tested and specimen geometry are largely related to the load capacity and resolution of the system and associated diagnostics. The upper bound of material ultimate strength σ_u that could be measured is dictated by yield of the bar/specimen bearing surfaces. Assuming that only normal stress is generated at the points of contact, yield at the bearing surfaces of the bar is predicted when $\sigma_u = \frac{1.5}{w}\sigma_{ys}$, where σ_{ys} is the uniaxial yield strength of the bar material, and w is the width of the specimen gage section in millimeters. For the current specimen and bar geometries samples with ultimate strength up to 900 MPa could be tested. Higher strength samples could be tested by further reducing the gage section width. The lower bound of sample material strength measurement is limited by the strain sensing capabilities of the current system. Based upon the signal to noise ratio the measured strain signals, it

Fig. 6 Engineering strain rate as a function of time

should be possible to accurately resolve materials with flow stresses as low as 10 MPa. This lower limit could be increased by reducing the cross section of the bars, or by increasing the sample cross section dimensions. Other diagnostic methods such as quartz force transducers [7] and optical interferometers [13] could be employed if finer force resolution is required.

Limitations also exist on the strain rate and strain levels that can be applied to the specimen. The upper bound of strain rate is largely dependent upon the maximum amplitude of the incident wave that can be supported without yielding the bar material. In the limiting case of a very weak sample the incident and reflected strain signals will be nearly identical. Assuming a yield strength of 300 MPa for the bars and a 1 mm gage length, Eq. (5) predicts a maximum strain rate of 42,500 s^{-1}. Specimens of finite strength will tend to reduce the maximum attainable strain rate slightly. Higher strain rates can be achieved by reducing the sample gage length, but the effects of compliance of the grip section of the specimen become more significant as gage length is reduced. We expect that gage sections shorter than 0.5 mm will not be practical for testing in the current apparatus.

Another factor limiting the maximum applied strain rate is the rise time required to achieve force equilibrium and constant strain rate deformation, as discussed in "Dynamic Tensile Flow Stress Measurements" section. While not a direct limitation, the strain accumulates in the specimen during the time to equilibrate and reach constant strain rate deformation is proportional to the applied strain rate. Assuming a linear ramp to constant strain rate in the sample $\dot{\epsilon}_{avg}$, the strain accumulated before constant rate is achieved is approximated as $\epsilon_{noneq} = \frac{1}{2}\dot{\epsilon}_{avg}t_{rise}$. Strains of up to 20 % are predicted to accumulate during the rise to constant strain rate conditions by using the maximum strain rate predicted above and the measured rise times of $\sim$10 µs, thus limiting the amount of useful data to only extremely large strain values. The rise time of the incident strain pulse is believed to result from the time it takes for the wave to equilibrate through the threaded connection. This section of the bars has a higher impedance than the other sections, and it takes several reflections for the stress to "ring-up" to equilibrium. Redesigning of this connection to minimize the length of the connection and the impedance mismatch to the other sections of the bars may reduce the rise time and extend the useful range of the system.

Summary and Conclusions

A miniaturized tensile Kolsky bar has been developed to facilitate the testing of metallic foils subjected to tensile loading at strain rates on the order of 10^4 s^{-1}. This bar incorporates recent developments in Kolsky bar testing

such as a hollow launch tube that houses an internal striker to provide a stable support for the bar components and allow for the use of traditional pulse shaping techniques. Bars of rectangular cross section with integrated sample gripping pockets are used to facilitate specimen mounting/alignment while minimizing disturbances to the 1-D wave propagation that may occur with grips that add significant mass to the system.

Capabilities of the system have been demonstrated by measuring the dynamic tensile constitutive response of 99.9 % magnesium samples at strain rates up to 10^4 s^{-1}. Conditions required for valid test results such as force balance across the specimen and constant strain rate deformation have been verified by analyzing the strain signals collected from the bars.

The miniaturization of the system provides several key benefits. The smaller sample dimensions allow for higher strain rates to be achieved. The smaller samples also allow for the deformation and failure processes to be observed on a smaller scale (while still viewing the entire specimen), providing a more fundamental understanding of the critical processes active during deformation. The system is also portable allowing for it to be easily transported to facilities offering advanced analytic capabilities, e.g. in-situ X-ray diffraction at the Advanced Photon Source at Argonne National Lab [18, 19]. The authors hope that this technique will provide a path forward for understanding mechanical response at the mesoscale.

References

1. Kolsky H (1949) An investigation of the mechanical properties of materials at very high rates of loading. Proc Phys Soc Sect B 62:676–700
2. Knezevic M, Levinson A, Harris R, Mishra RK, Doherty RD, Kalidindi SR (2010) Deformation twinning in AZ31: influence on strain hardening and texture evolution. Acta Mater 58(19):6230–6242
3. Hartley KA, Duffy J, Hawley RH (1985) The torsional Kolsky (split-Hopkinson) bar. ASM Metals Handb 8:218–228
4. Staab GH, Gilat A (1991) A direct-tension split Hopkinson bar for high strain-rate testing. Exp Mech 31(3):232–235

5. Huang H, Feng R (2004) A study of the dynamic tribological response of closed fracture surface pairs by Kolsky-bar compression-shear experiment. Int J Solids Struct 41(11):2821–2835

6. Jia D, Ramesh KT (2004) A rigorous assessment of the benefits of miniaturization in the Kolsky bar system. Exp Mech 44(5):445–454

7. Cheng M, Chen W, Weerasooriya T (2005) Mechanical properties of Kevlar KM2 single fiber. J Eng Mater Technol 127(2):197–203

8. Sanborn B, Foster M, Moy P, Weerasooriya T (2014) Microtensile Experimental Methods to study the Dynamic Behavior of Thin Metallic Films. In Song B, Casem D, Kimberley J (eds) Dynamic behavior of materials, volume 1, conference proceedings of the society for experimental mechanics series. Springer, New York

9. Ramesh KT (2008) High strain rate and impact sxperiments. In: Sharpe W Jr (ed) Springer handbook of experimental solid mechanics, chapter 33. Springer, Berlin, pp 929–960

10. Gray GT (2000) Classic split-Hopkinson bar testing. In: Kuhn H, Medlin D (eds) ASM handbook volume 8: mechanical testing and evaluation. ASM International, Materials Park, pp 462–476

11. Guzman O, Frew DJ, Chen W (2011) A Kolsky tension bar technique using a hollow incident tube. Meas Sci Technol 22(4):045703

12. Song B, Antoun BR, Connelly K, Korellis J, Lu WY (2011) Improved Kolsky tension bar for high-rate tensile characterization of materials. Meas Sci Technol 22(4):045704

13. Casem DT, Grunschel SE, Schuster BE (2012) Normal and transverse displacement interferometers applied to small diameter Kolsky bars. Exp Mech 52(2):173–184

14. Watson RB (2008) Bonded electrical resistance strain gages. In Sharpe WN Jr (ed), Springer handbook of experimental solid mechanics, chapter 12. Springer, New York, pp 283–334

15. Furukawa M, Horita Z, Nemoto M, Langdon TG (2001) Review: processing of metals by equal-channel angular pressing. J Mater Sci 36(12):2835–2843

16. Krywopusk NM, Kecskes LJ, Weihs TP (2015) Characterization of the microstructure of pure Mg and AZ31B processed by ECAE. Manuscript in preparation

17. Davies EDH, Hunter SC (1963) The dynamic compression testing of solids by the method of the split Hopkinson pressure bar. J Mech Phys Solids 11(3):155–179

18. Lambert PK, Hustedt CJ, Vecchio KS, Huskins EL, Casem DT, Gruner SM, Tate MW, Philipp HT, Woll AR, Purohit P et al (2014) Time-resolved X-ray diffraction techniques for bulk polycrystalline materials under dynamic loading. Rev Sci Instrum 85(9):093901

19. Hudspeth M, Sun T, Parab N, Guo Z, Fezzaa K, Luo S, Chen W (2015) Simultaneous X-ray diffraction and phase-contrast imaging for investigating material deformation mechanisms during high-rate loading. J Synchrotron Radiat 22(1):49–58